Grinding performance of MgF_2 ceramics using biomimetic shark fin grinding wheels with different structure parameters

Xiaohong Zhang[a,b,*], Ziyi Zhou[a,c], Dongdong Wen[a,c], Zhaoyao Shi[d], Xun Chen[b], Xiong Tang[e], Wentao Rong[a,c], Tianzhongsen He[a,c]

[a]College of Mechanical Engineering, Hunan Institute of Science and Technology, Yueyang, 414006, China;

[b]Advanced Manufacturing Technology Research Center, Liverpool John Moores University, Liverpool, 999020, UK;

[c]Key Laboratory of Intelligent Manufacturing and Service Performance Optimization of Laser and Grinding in Mechanical Industry, Yueyang, 414006, China;

[d]Beijing Engineering Research Center of Precision Measurement Technology and Instruments, Beijing University of Technology, Beijing 100124, China.

[e]College of Mechanical and Electrical Engineering, Yueyang Vocational Technical College, Yueyang, 414000, China;

*Corresponding author. E-mail address: jansbomb@126.com.

Abstract

In the field of precision machining, with the popularity of brittle and hard materials such as infrared windows, it has become difficult for conventional diamond grinding wheels to effectively perform high-quality machining. The structuring of traditional diamond grinding wheels using a pulsed laser is a key technology to effectively improve the grinding quality of grinding wheels. In this paper, three new shark fin diamond grinding wheels (SFSGW) with different slot widths are designed based on the excellent drag-reducing and channelizing properties of shark dorsal fins. The grinding performance of traditional grinding wheels (USGW) and SFSGW on magnesium fluoride ceramics was compared. The effects of SFSGW on the surface quality, surface roughness and wheel damage of the workpiece were investigated. The results showed that the surface roughness of ceramics after grinding by SFSGW was reduced by 22.15% compared with USGW, and the surface quality was better. Proper construction increases the material removal rate of the wheel and improves the wear resistance and service life of the wheel.

Keywords: Precision machining; Shark fin-like structure; Laser processing; MgF_2 ceramics; Surface roughness; Wear resistance.

1. Introduction

Infrared transparent ceramics is the latest development of infrared optical materials, due to its low porosity, high densities, wide transmission band and extremely high-temperature resistance, it has become the main material for the window and fairing of infrared devices such as various types of aircraft and detectors, with the role of transmitting target signals, maintaining aerodynamic shape, and protecting internal components [1]. Magnesium fluoride (MgF_2) has an excellent combination of properties such as low refractive index coefficient, corrosion resistance, excellent thermal stability and hardness, as well as the lowest linear refractive coefficient and light scattering properties, which makes it an excellent infrared window material [2-4]. Magnesium fluoride ceramics have been widely used in infrared guidance, infrared imaging guidance and other fields [5]. However, polycrystalline magnesium fluoride ceramics are typically brittle materials because they are susceptible to surface microscopic chipping, cracking, and grain pullout during processing [6]. Brittle and hard materials are characterized by high hardness and brittleness, and these materials are prone to fracture or chipping when they are subjected to external forces, rather than deformation as in the case of plastic materials. Therefore, when using traditional tools for cutting, the tool is easily damaged by large impact and thermal stress, while the machining surface is also prone to cracks, chipping and other defects, and this damage will affect the processing efficiency. Grinding wheel machining can reduce surface cracks, chipping defects, and improve machining quality. Therefore, the ultra-precision grinding method remains the mainstream machining method for processing brittle hard ceramics such as polycrystalline magnesium fluoride [7].

Ultra-precision grinding is a machining method for machining materials such as aluminum oxide and silicon carbide by using super-hard abrasive wheels such as synthetic diamond and cubic boron nitride as abrasive tools to obtain a surface with nanometer-level roughness. As the demand for hard and brittle materials increases dramatically, how to obtain high-quality material surfaces quickly has become the focus of research. Structured grinding wheels are increasingly recognized as a promising technology for enhancing the grinding performance of materials. Surface texturing techniques are also widely used in various engineering devices such as thrust bearings [8-10], cutting tools [11-13], cylinder liners and piston rings [14-16]. Wu et al [17] used a pulsed laser to generate microstructures on the appearance of a traditional grinding wheel with high shape accuracy and small sidewall inclination, and the use of this wheel to grind SiC was found to inhibit the brittle removal of the material, reduce the number of cracks, and obtain a nano-scale surface roughness. Guo et al [18] produced a new micro-structured grinding wheel for grinding optical glass by ablating microgrooves of different depths on the appearance of a traditional grinding wheel with a nanosecond pulsed laser technique. Experiments showed that the micro-structured grinding wheel had a better chip-holding effect. The normal and tangential forces during the grinding process were significantly reduced, and there were smoothing traces at the tip of the abrasive grains and at the side edges of the microstructure, confirming that the microstructure played an effective role in the grinding process. Chen et al [19] used pulsed laser technology to accurately ablate the leaf vein structure onto the appearance of a bronze-bonded diamond grinding wheel and analyzed the effect of the leaf vein bionic wheel on the air reflux and pressure on the SiC ceramic surface during the grinding process by simulation. A series of grinding experiments were conducted to compare the grinding performance of the bionic and conventional grinding wheels on hard and brittle ceramics. The experiments show that the normal and tangential grinding forces of the structured wheel on SiC ceramics are reduced by 47.37% and 41.06%, respectively, compared with those of the conventional wheel, and the surface roughness is reduced by nearly 30%.

Bionics, encompassing the examination of the structure and function of diverse organisms, aims to decipher their operational principles and integrate them into various engineering technologies to address or enhance a myriad of engineering challenges [20-22]. In the realm of bionic noise and drag reduction, Ye et al. [23] investigated the morphological structure of shark fins and applied it to the design of side-view mirror shells. Subsequently, numerical simulations were conducted to ascertain the flow field distribution behind the side-view mirror, followed by validation through wind tunnel testing. The findings indicate that, in comparison to the standard model, the incorporation of bionic shark fin structures effectively streamlines airflow, leading to a significant enhancement of the flow field and a reduction in aerodynamic noise. Wu et al [24], in order to solve the problem of the non-smooth leading edge of the wing of a long-eared owl, investigated and designed eight types of worm shell tongue structures to reduce the aerodynamic noise of a centrifugal fan and numerically simulated its flow and sound characteristics. The results show that the noise of the fan with the bionic structures is reduced by 1.5 dB compared to the fan without structures, and the mass and flow rate are increased.

Shark fins play a very important stabilizing role as the shark swims at high speed. The shark dorsal fin is triangular in the horizontal plane, and this structure can split the water flow during the shark swimming, fully reducing the viscous drag and inhibiting the wake separation. The bionic application of the shark fin is also very extensive, Y. Zhang et al [25] designed a new type of spoiler by studying the shape of the shark's fin, and through the wind tunnel test, it was concluded that the bionic structure can inhibit the formation of turbulence, weaken the airflow separation of the rear wake, improve the structure of the flow field, so as to achieve the purpose of reducing the vehicle's aerodynamic drag. Wei C et al [26] used the shape of a shark dorsal fin as a new type of bionic nozzle runner designed, and through simulation as well as physical experiments, it is concluded that the bionic nozzle has good anti-clogging performance and reasonable hydraulic performance. The particle passage rate of the bionic emitter was improved by 37.6% compared to the conventional emitter.

This paper presents the design of a bionic grinding wheel featuring a shark fin structure, inspired by the morphological characteristics of the dorsal fin of sharks. Initially, an extensive literature review was conducted to identify a mathematical model resembling a double U structure akin to that of a shark fin [27], which was then refined through Python software. Subsequently, the geometric model of the bionic structure was derived from the mathematical framework, followed by the creation of a corresponding geometric pattern using Computer-Aided Design (CAD) software, which was subsequently transferred to the laser processing system. Following a series of orthogonal experiments, the bionic structure was meticulously ablation onto the surface of the grinding wheel utilizing selected laser parameters. Three bionic grinding wheels inspired by shark fins, each possessing varying slot widths, were crafted and subsequently subjected to comparative grinding experiments against conventional grinding wheels. The surface morphology and surface roughness of MgF_2 ceramics after a certain grinding depth by different grinding wheels, as well as abrasive grains breakage by different grinding wheels are discussed.

2. Experimental section

2.1 Shark fin bionic grinding wheel preparation process

2.1.1 Geometric parameter design of shark fin structure

Sharks exhibit remarkable agility as they traverse through aquatic environments, heavily relying upon the structural integrity of their dorsal fins to maintain stability during locomotion. The dorsal fin of the shark presents with a flattened apex anteriorly, while its dimensions progressively augment both in height and thickness along the dorsal spine. Analyzed from the perspective of fluid dynamics, this special structure changes the structure and velocity distribution of the turbulent layer on the skin surface of the shark when swimming, suppressing the turbulent pulsation of the attached surface layer, thus reducing the frictional resistance and having the flow characteristics of low flow resistance [28]. Furthermore, the patterning of the shark fin embodies a fractal architecture, heightening water pressure and velocity at the nexus of flow channels. Therefore, the shark fin structure utilized on the grinding wheel can have the advantages of lubricating the grinding area, reducing the grinding temperature, and improving the chip removal efficiency. The shark fin is shown in Fig. 1.

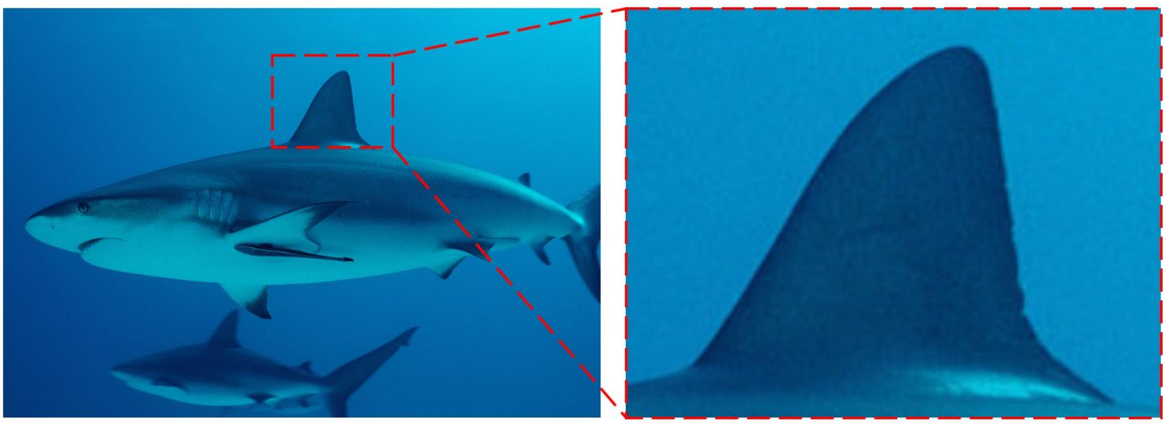

Fig. 1. Shark fin morphology.

In this experiment, an in-depth study of the shark morphology structure was utilized to successfully design a bionic structural model with excellent drag reduction and chip removal properties. The bending structure has good stability in practical applications and meets the requirements of practical engineering applications such as energy absorption. Among them, Fig. 2 demonstrates the mathematical model of the shark fin structure, which consists of two different trigonometric functions (Eqs. (1) and (2)). In the mathematical model, h_1 and h_2 denote the amplitudes of curves 1 and 2, respectively. $2l$ is the length of the horizontal projection of the curve. Based on the equal scale design, we defined the dimensional parameters h_1, h_2 and l of the mathematical model as 10, 4 and 5, respectively, and carried out the preliminary drawing of the mathematical model using CAD software.

$$y_1 = -\frac{h_1}{2}\cos\frac{\pi x_1}{l} \quad (1)$$

$$y_2 = -\frac{h_2}{2}\cos\frac{\pi x_2}{l} \quad (2)$$

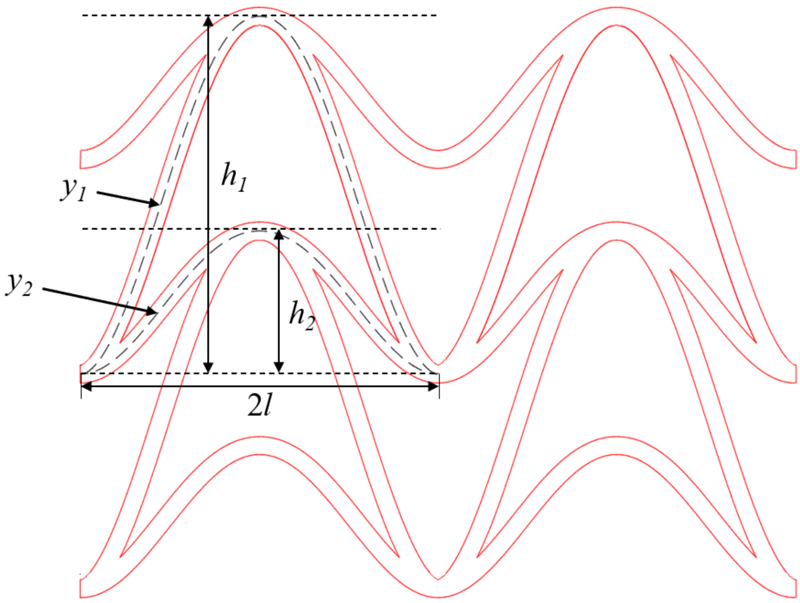

Fig. 2. Geometric model of shark fin.

As an innovative grinding tool, bionic grinding wheels have shown great promise and significant value in project applications and academic research. Theoretical mathematical modeling of bionic structures must be effectively integrated with real-world applications in engineering for practical implementation. According to the specific parameters, the geometrical parameters of the imitation shark fin micro-groove structure need to be specifically designed. In this study, the dimensional parameters of the micro-groove structure are meticulously tailored to align with both the parameters of the grinding wheel and the mathematical model. Utilizing Solid Works software, we integrate the precise dimensions of the grinding wheel with the geometric specifications of the shark-fin structure, resulting in the successful creation of a shark-fin-like structure suitable for the grinding wheel. The fractal structure can enhance the internal hydraulic pressure of the runners and effectively promote the flow of coolant in the runners and the transfer of grinding heat. In order to increase the number of internal runners and fractal structures, this paper proposes to form a shark fin bionic structure by combining two positively aligned shark fin structures and one reversely aligned shark fin structure. The geometrical model is shown in Fig. 3.

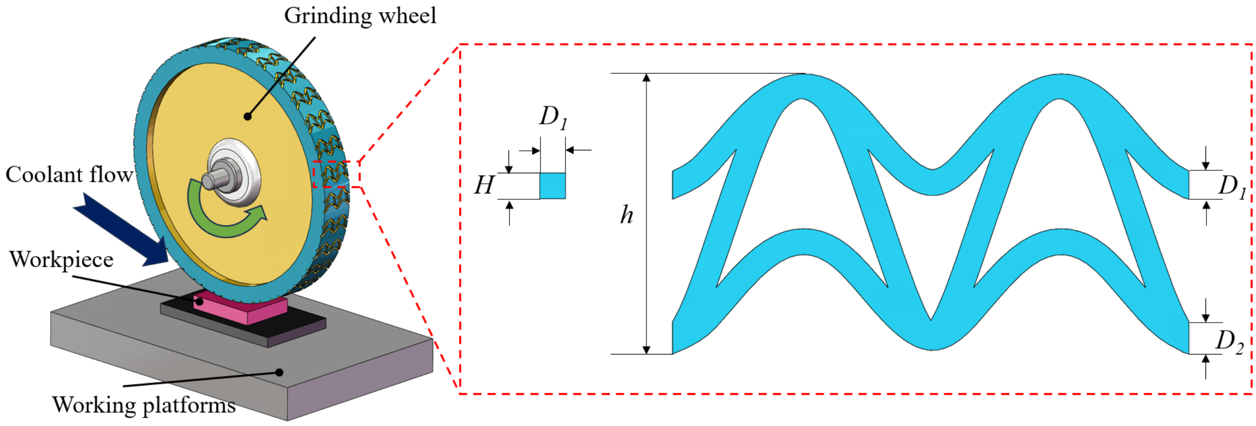

Fig. 3. Structural parameters of shark fin.

The geometric dimensions of the shark-fin-like structure include the slot width D_1, the intersection width of two grooves D_2, the total height of the shark-fin h and the slot depth H. In order to avoid too large a structured area, which could lead to a significant reduction in the service life of the wheel, the shark fin structure will not cover the entire appearance of the wheel. The grinding wheel used in this article is the bronze bond diamond grinding wheel produced by Zhengzhou Abrasives Research Institute. There are other common bond grinding wheels such as resin bond grinding wheels and rubber bond grinding wheels, etc. Metal bond diamond wheels have better abrasion resistance and thermal conductivity, making them more suitable for processing hard and brittle materials such as MgF_2 ceramics than other bond wheels. The bronze bond grinding wheel has a diameter of 200 mm, a width of 20 mm, an abrasive thickness of 5 mm and a mesh size of 100. The depth of the structural groove H should be less than the thickness of the abrasive material 5mm, in order to control the variables, the depth of the structural groove designed uniformly in this paper is 0.9mm. The geometric width of the shark-like fin structure should be 20mm. The bionic structures designed in the previous were overlaid on the appearance of the grinding wheel with the central of the wheel circle as a reference, and the spacing between each group of structures was 12°, for a total of 30 groups. In order to investigate the effect of structured area and groove width on the grinding performance of the grinding wheel, three shark fin structures with different slot widths were designed in this paper. Setting the maximum slot width to 1 mm is to prevent the structured area of the grinding wheel from being too large, which leads to too few effectively processed abrasive grains and reduces the grinding efficiency of the grinding wheel. Table 1 demonstrates the structuring parameters for different slot widths.

Table 1 Parameters of each shark fin-like structure

	Structure 1	Structure 2	Structure 3	Unstructure
D_{1}(mm)	1	0.75	0.5	/
D_{2}(mm)	1.27	0.89	0.58	/
H(mm)	0.9	0.9	0.9	/
h(mm)	10	10	10	/

2.1.2 Laser experiments

The laser beam has good optical uniformity, and its optical properties can remain stable during the transmission process, which facilitates precise processing and imaging. Typically, the desired structure is accurately machined onto the diamond grinding wheel using the laser galvanometer system in the laser system. This section describes the process of irradiating the appearance of a grinding wheel with a laser beam and removing the surface material by ablation to create a structured grinding wheel. First, the designed shark fin imitation model was introduced to import the laser apparatus. Then the side edges of the wheel were marked at 12° intervals, and the grinding wheel was rotated at 12° after each ablation to carry out the next ablation experiment. Finally, all the thirty structures were accurately ablated to the appearance of the grinding wheel. Fig. 4 shows the experimental platform for laser processing used in this experiment. The laser equipment is an LS150QC-50F-1 millisecond pulsed laser, and the average power of laser processing is 1-50W.

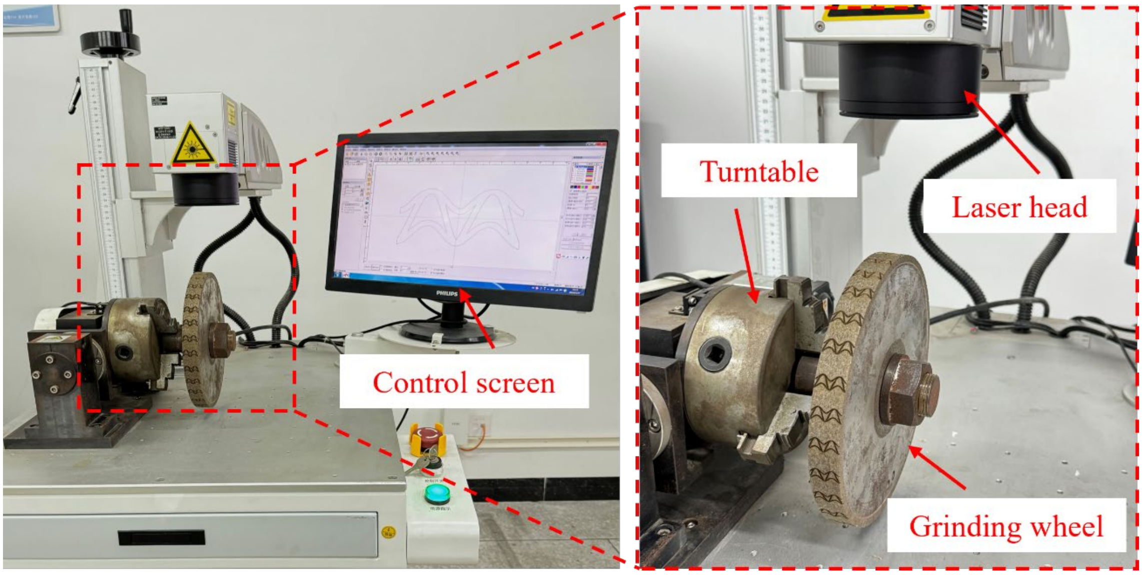

Fig. 4. Experimental apparatus for pulsed laser structured.

In the process of precision grinding, the diamond grains of the grinding wheel will gradually become blunt under the action of friction and extrusion. The abrasive debris generated by grinding will be embedded in the pores, which will reduce the diamond grinding wheel capacity of the diamond grinding wheel and cause the surface roughness of the workpiece to become larger, the grinding heat to rise, and the grinding accuracy to be reduced. Therefore, before the laser experiment starts, the grinding wheels should be mounted to the grinder in sequence and precisely dressed with green silicon carbide oil stone. Green silicon carbide oil stones are fluffy, very tough and have good abrasive self-sharpening properties. It is often used to polish dulled abrasives, restoring the dulled abrasive to a new cutting edge. This experiment consists of a high-precision PI four-degree-of-freedom moving stage that forms the transmission system. Once the formal experiment started, the efficiency of laser utilization was improved by the installation of an electric spindle on the machining platform, which enabled the grinding wheel to rotate accurately and stably during the laser machining process. In the laser processing experiment, the too-low laser power will make the processing efficiency low, the material processing depth is not enough and other problems, while the laser power is too high will make the surface of the grinding wheel carbonization is serious, so as to reduce the grinding ability of the grinding wheel. Prolonged high-power work will also cause damage to the laser equipment and other problems. Too high a laser pulse frequency will make the laser beam on the material residence time become shorter, resulting in the cutting surface becomes uneven. Too low a pulse frequency will make it difficult for the melting and vaporization of the material on the surface of the grinding wheel to form quickly, which may lead to uneven structured grooves on the edges and reduce the quality of the cut. After a series of laser processing orthogonal experiments, the laser frequency, power, scan time and other laser processing parameters are continuously adjusted, and finally the optimal laser parameters suitable for the processing of diamond grinding wheels in this paper are obtained, as shown in Table 2. Optimal laser parameters allow for precise ablation of the designed structural dimensions onto the grinding wheel surface, successfully producing a bionic diamond grinding wheel.

Table 2 Optimum laser-structured parameters

Laser processing parameters	Values
Spot size d_f (mm)	0.06
Pulse frequency f (kHz)	25
Laser power P (W)	20
Scan speed v_{ss} (mm/s)	1000
Number of laser ablation N	24

2.2 Grinding experiments

The workpiece samples utilized in the grinding experiments were MgF_2 ceramics obtained from Qijinxin Company, located in Quanzhou, China. Table 3 delineates their respective physical properties. The workpiece samples were characterized by dimensional parameters of 20 mm in length, 17 mm in width, and 5 mm in height. In the preparation for grinding, the magnetic suction block was firstly placed on a heater to be heated to the appropriate temperature. Next, paraffin wax was heated to a melted state and applied to the surface of the magnetic suction block. Subsequently, the MgF_2 ceramic is pasted onto the surface of the magnetic suction block, and when it cools down to the proper temperature, the ceramic will be firmly fixed on the magnetic suction block. Finally, the magnetic suction block with the workpiece is fixed on the working platform of the grinding machine using the magnetic force of the grinding machine to ensure the stability and accuracy of the workpiece during the grinding process. After testing the ideal wheel speed and linear speed, the grinding wheel was fed for the first time at a depth of 5 μm, and for the second time at 10 μm, in increasing increments. The surface morphology of the workpiece was observed after each feeding experiment. Each feed of the wheel needs to be separated by more than five minutes to ensure that there is no experimental error before the next feed test.

Table 3 MgF_2 ceramic properties

Material	Theoretical density (g/cm^3)	Vickers hardness (GPa)	Bending strength （MPa）
MgF_2 Ceramic	3.18	5.55	100

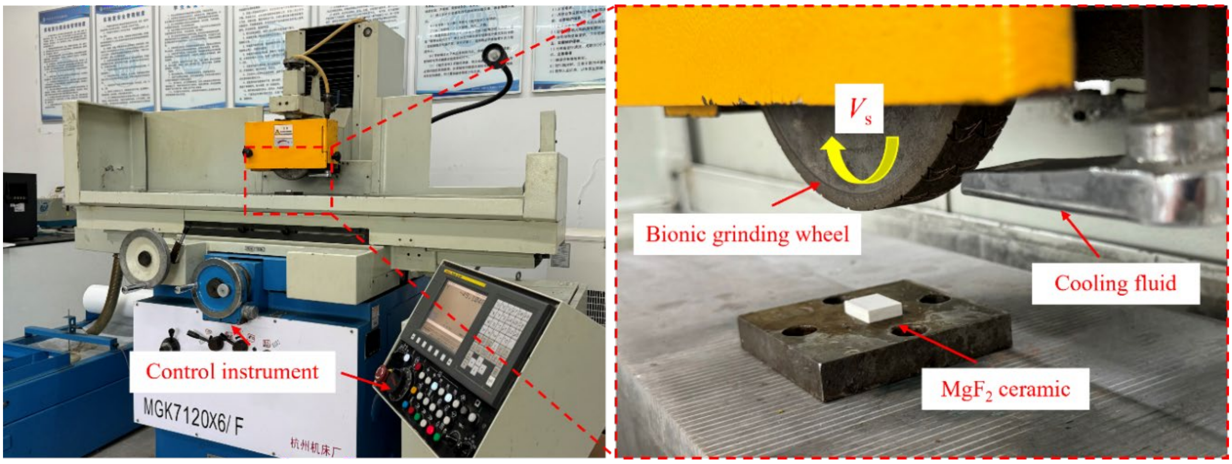

Fig. 5. Experimental setup of grinding experiment.

The most suitable grinding parameters were determined through several pre-experiments before the start of the experiment, as shown in Table 4. Pre-experiment designed a number of groups of grinding parameters and compared, the experiment found that when the grinding wheel feed rate is too slow will greatly reduce the grinding efficiency, making the workpiece and the grinding wheel friction time increases, affecting the surface roughness. And the feed rate is too fast will increase the friction and heat between the grinding wheel and the workpiece, causing damage to the workpiece. The grinding wheels used for the experiment were mounted on a CNC high-precision surface grinder

(MGK7120A), as shown in Fig. 5. The grinding fluid used in the grinding process is a 3% water-based coolant (type W20), which is injected into the contact area between the grinding wheel and the MgF_2 ceramic at a rate of 25 liters per minute. To mitigate experimental discrepancies, multiple grinding experiments were conducted on various workpieces employing identical grinding parameters. Pre- and post-grinding assessments of the workpiece surface roughness were conducted using a three-dimensional laser scanning confocal microscope (OLYMPUS LEXT OLS5000), while the grinding wheel wear was examined using an ultra-depth-of-field microscope (VHX-5000). A comparative analysis of the grinding performance between three different slot widths of biomimetic grinding wheels (SFSGW) and conventional grinding wheels (USGW) was conducted.

Table 4 Parameters used while grinding MgF_2 workpiece

Grinding parameters	Value
Tools	Bronze-bond diamond grinding wheel
Type of grinding wheel	200 * 20 * 32.5 SD100
V_s (m/s)	30
a_p (μm)	5, 10, 15, 20, 25
V_w (mm/min)	2000
Grinding coolant	Water-based coolant (Type W20)
Grinding mode	Down-grinding

3. Experimental results and discussion

3.1 Surface topography of SFSGW after laser processing

Laser ablation is the process of removing solid surface materials by heating and sublimation of the surface materials through laser beam irradiation, which causes the surface materials to absorb the laser energy. During laser processing, the effective power density (I_A) of the laser beam on the appearance of the grinding wheel dictates the efficacy of material removal [29], a higher effective power density (I_A) corresponds to a greater surface material removal rate. Which is defined as Eqs. (3):

$$I_A = \eta \frac{P_{avg}}{S} \tag{3}$$

In the formula, η represents the absorption rate of laser energy by the material on the appearance of the grinding wheel; P_{avg} denotes the average laser power; and S signifies the effective irradiated area on the appearance of the grinding wheel during the laser processing of the diamond grinding wheel [30].

Given the consistent laser parameters employed throughout this paper's laser experiments, both the average laser power (P_{avg}) and the effective irradiated area (S) remain constant variables for this study. Consequently, the effective power density (I_A) of laser irradiation on the grinding wheel's surface is influenced by the absorption rate (η) of laser light by the material. Due to the higher laser energy absorption rate of the bronze metal bond on the grinding wheel's appearance compared to that of the diamond abrasive grains, the laser's effective power density is unevenly distributed on the grinding wheel, leading to a faster removal rate of the bronze bond than that of the diamond abrasive wheel [31]. By observing the surface morphology of the bionic grinding wheel in Fig. 6, it can be observed that there are a large number of scintillating particles at the bottom of the groove of the grinding wheel, which are the diamond particles that have not been removed by the laser.

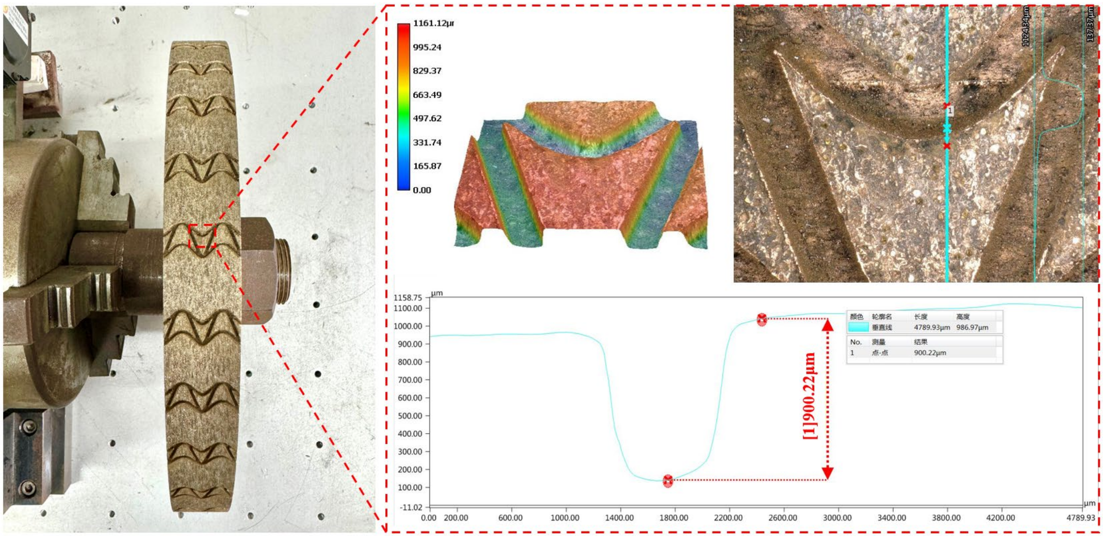

Fig. 6. Surface topography of the diamond grinding wheel after the laser imitation shark fin structured.

Fig. 6 shows the micro-morphology of the grooves after machining the bionic shark fin texture onto the surface of grinding wheel using a millisecond laser. As depicted in the figure, a discernible slope is evident on the sidewalls of both sides of the groove, attributed to the Gaussian distribution of laser energy. This distribution entails a variation in light intensity across the cross-section, with a significant decline in energy density observed in the peripheral regions distant from the spot center. Consequently, this phenomenon results in a diminished ablation effect on the material at the groove's edge. The magnitude of the increase in the groove depth decreases with the increase in the time that the laser experiments are carried out because when the laser ablates the grinding wheel for a sufficiently long period of time, the metal bond at the bottom of the groove melts at a rate greater than the rate of gasification and evaporation. The molten metal material will react with the oxygen in the air as it melts and cools, causing the material's absorption rate of the laser energy to change, and thus it will become more difficult to remove. From the figure, it can be seen that some metal elements have been oxidized and turned into black melt, which cools and adheres to the bottom of the groove.

3.2 Surface morphology and roughness of MgF_2 ceramic after grinding

3.2.1 Surface morphology

There are many factors that determine the surface morphology of the materials, such as grinding tools, grinding parameters (grinding wheel speed, cutting depth, etc.), and the degree of wear of the processing tools. In precision machining, the surface quality of the materials after processing is usually represented by surface roughness and surface morphology. This section uses the same grinding parameters to grind MgF_2 ceramics with four different grinding wheels, and then observes and compares the surface morphology and roughness of the ground MgF_2 ceramics using a laser confocal microscope.

Fig. 7 illustrates the surface morphology of MgF_2 ceramics under the influence of various grinding wheels and diverse grinding depths. The bionic wheel did not reach the maximum deformed chip thickness in this experiment at a grinding depth of 5 μm, and it was observed that the removal manner of material from the surface of the workpiece was mainly plastic removal, with a small amount of brittle fracture occurring on the surface of ceramics processed with the conventional wheel. Compared with the other two bionic grinding wheels, the structural area of structure 3 SFSGW is smaller and the grinding stress on the workpiece surface is higher, so that the ceramics processed with the structure 3 SFSGW show obvious abrasive scratches and small pits on the surface after grinding. In contrast, structure 2 SFSGW displayed a negligible presence of abrasive scratches.

At a grinding feed depth of 10 μm, notable abrasive scratches of considerable depth emerged on the ceramic surface subsequent to the grinding process with structure 1 SFSGW. This occurrence can be attributed to the compromised surface integrity of structure 1 SFSGW, which engaged the fewest effectively processed abrasive grains during the grinding. Consequently, the abrasive grains that were effectively machined encountered the highest grinding stress throughout the grinding operation, culminating in the formation of deep scratches. As the griding depth increases, the surface material removal of MgF_2 ceramics ground by SFSGW begins to show a plastic/brittle transition at a griding depth of 15 μm. USGW Large areas of brittle removal begin to appear on the surface of the workpiece.

The larger craters in the USGW and structure 3 SFSGW at grinding depths of 20 μm and 25 μm are due to the fact that the volume of diamond debris and abrasive debris generated by grinding increases with the depth of grinding during the grinding process. Since USGW does not have good chip removal capability, the chips generated by grinding repeatedly rub against the workpiece in the grinding area, resulting in rapid destruction of the surface morphology of the workpiece. Structure 3 SFSGW structure grinding performance is not significantly improved, and the ceramic surface quality after grinding is comparable to that of USGW. From a grinding depth of 20 μm onwards, the removal of material from the surface of the workpiece by the bionic wheel becomes brittle removal, as the depth of cut has reached the maximum deformation depth of cut, and the structuring is no longer able to counterbalance the grinding forces generated by the feed depth. Compared to structure 3 SFSGW and USGW, structure 2 SFSGW has good chip evacuation properties and also effectively reduces the grinding heat generated during grinding. Compared with structure 1 SFSGW, structure 2 SFSGW has less grinding stress on individual abrasive grains during grinding, better wear resistance performance of the grains, and more grains that can be efficiently processed. As the machining depth increases, the abrasive grains of structure 1 SFSGW wear more, and the surface morphology of its workpiece deteriorates. Through observation, it can be found that structure 2 SFSGW has the best surface morphology of the workpiece after grinding. MgF_2 ceramics, as a representative material of porous ceramics, generate a lot of pores during the production process, and therefore some traces of pores exist on the surface of the ceramics after grinding.

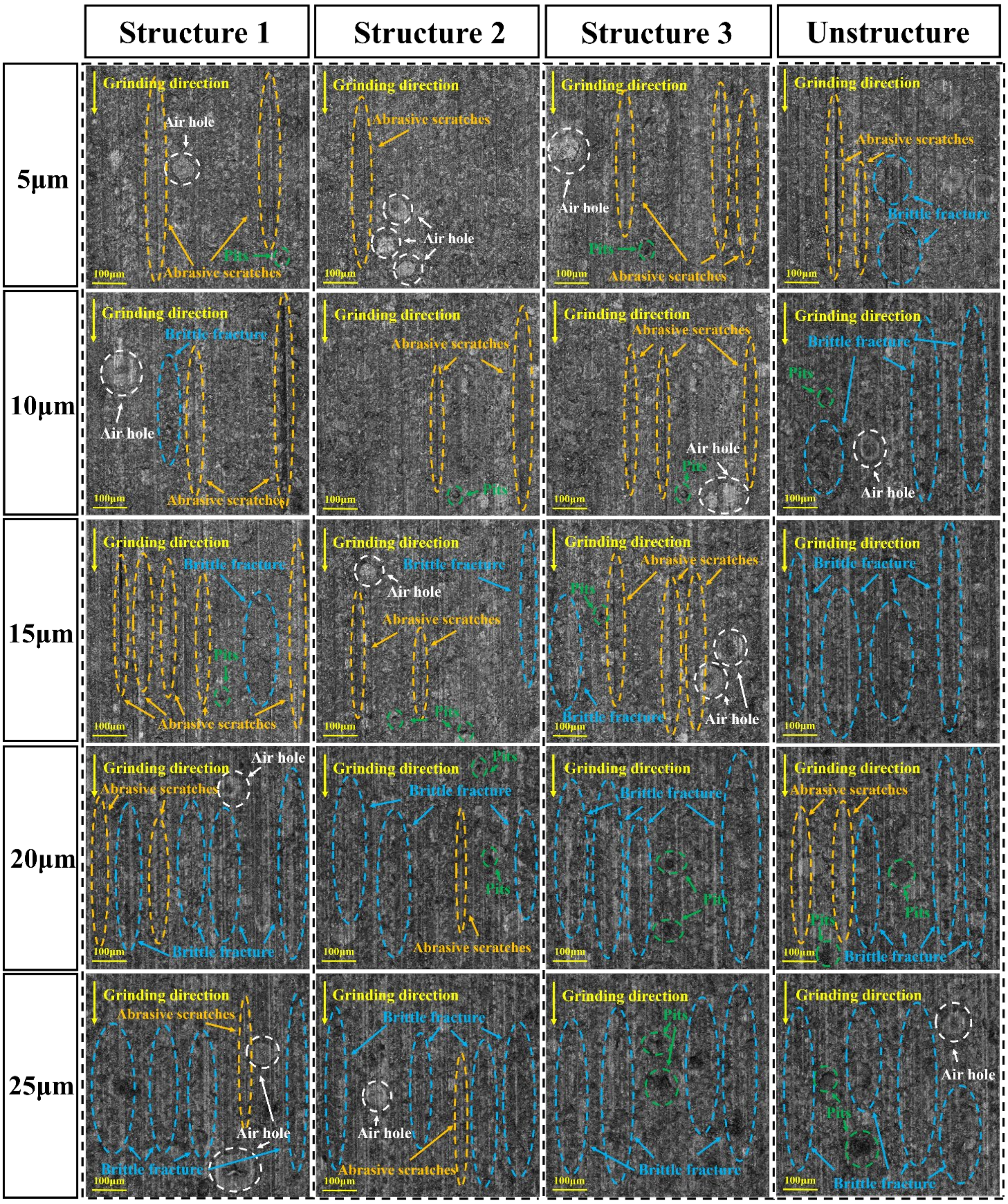

Fig. 7. Surface morphology of MgF_2 ceramics after grinding.

3.2.2 Surface roughness

The evaluation parameters of surface roughness are generally divided into two-dimensional evaluation parameter R_a and three-dimensional evaluation parameter S_a. As the traditional two-dimensional parameter R_a only utilizes very limited information on the surface, it cannot exclude the intrinsic influence of deep holes and cracks, and the measurement stability is low. And the results of surface roughness in different directions and positions have a large gap, resulting in the inability to comprehensively characterize the surface morphology of the workpiece. The three-dimensional parameter S_a can reflect the workpiece surface shape and performance characteristics more comprehensively, accurately and intuitively from the transverse and portrait directions. Therefore, this paper adopts S_a as the evaluation index of surface roughness of MgF_2 ceramics grinding by bionic shark fin grinding wheel. In statistics, data are usually collected using the five-point sampling method, in which five sample points are randomly selected to represent the whole population in order to understand the characteristics of the population more effectively. However, in high-precision numerical occasions, the five-point sampling method will produce a certain sampling error. Therefore, in this paper, the seven-point sampling method is chosen, in which each sampling frame consists of a square with a side length of 150 μm. This method has a wider sampling range, provides more data points, and helps to reduce the influence of extreme values or outliers.

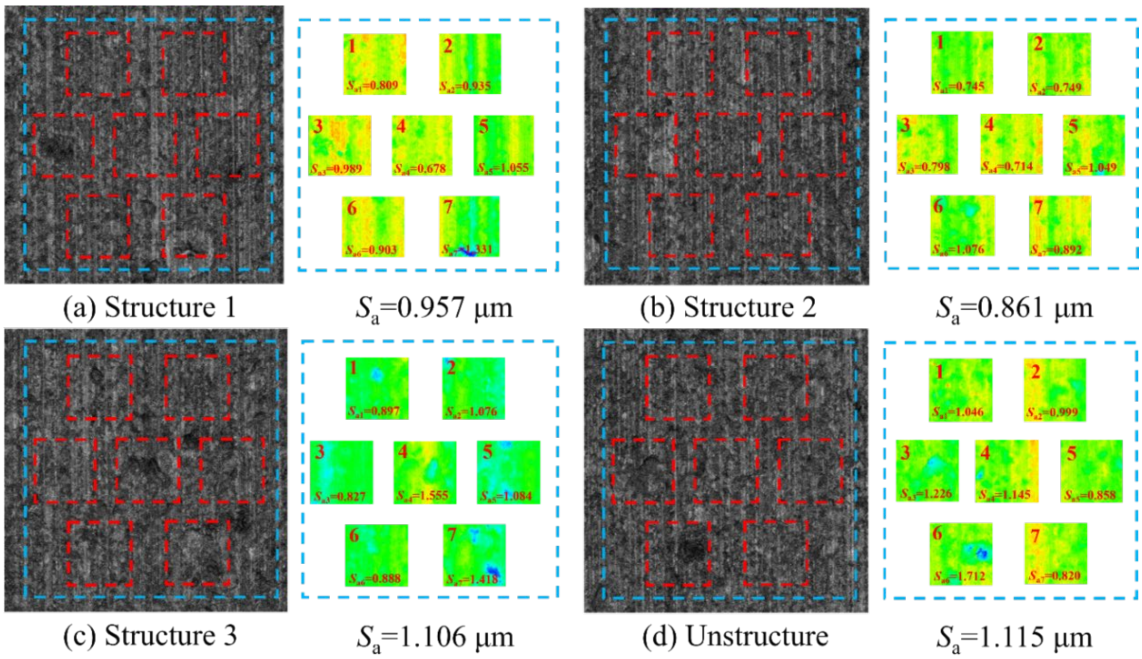

Fig. 8. Surface roughness of MgF_2 ceramics after grinding.

Fig. 8 shows the difference in the surface roughness of the workpiece after being ground by the bionic shark finned and the conventional diamond grinding wheel at a depth of cut of 25 μm. The surface roughness of the ceramic after grinding by the conventional wheel is the largest, and the surface roughness of the ceramic after grinding by the structure 2 SFSGW is the smallest. The surface morphology of the workpiece and surface roughness are closely related, the traditional grinding wheel does not have the good lubrication performance of the structured wheel, with the increase of the grinding time, the increase of the grinding temperature, the abrasive chips are more difficult to be discharged from the grinding area so that the surface roughness increases sharply. During the fabrication of structured grinding wheels, the surface integrity of the wheel decreases as effectively processed abrasive grains are removed from the surface of the wheel, and there is no significant improvement in the abrasive performance of the wheel until a certain threshold is reached in the infusion and chip removal capabilities of the structured wheel. Therefore, the three-dimensional surface roughness S_a of the MgF_2 ceramics after USGW grinding is 1.115 μm, and the three-dimensional surface roughness S_a of the MgF_2 ceramics after structure 3 SFSGW grinding is 1.106 μm, which is only 0.81% lower than that of USGW. The three-dimensional surface roughness S_a of the MgF_2 ceramics after grinding of structure 1 and 2 SFSGW is 0.957μm and 0.861μm, which is 11.84% and 22.15% lower than the USGW, respectively. Fig. 9 demonstrates the connection between the surface roughness of the workpiece and the depth of grind after grinding MgF_2 ceramics with different bionic and conventional grinding wheels. The three-dimensional surface roughness Sa increases with the increase of grinding depth of the wheel, and the overall surface of the workpiece after grinding by the bionic grinding wheel is superior to that of the conventional grinding wheel. The three-dimensional surface roughness S_a was 0.682±0.03 (Structure 1 SFSGW),0.653±0.03 (Structure 2 SFSGW),0.726±0.03 (Structure 3 SFSGW) and 0.793±0.03 (Untructure) when the depth of cut was 5μm. The S_a of the workpiece was reduced by 13.99% for structure 2 SFSGW compared to USGW. Combined with the previous description of the surface morphology section, it can be seen that structure 2 SFSGW has the best work surface morphology and surface roughness after grinding.

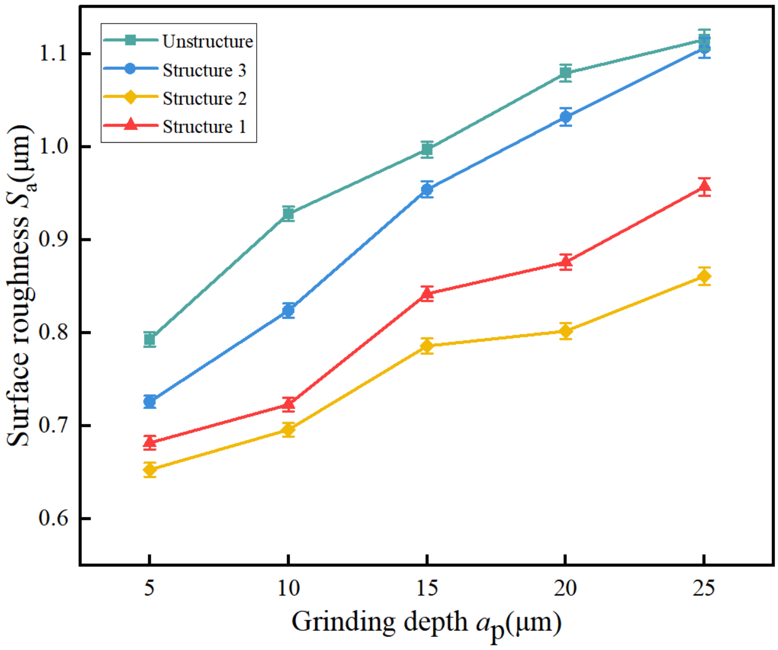

Fig. 9. Effects of grinding depth on surface roughness.

3.3 Workpiece edge damage

Fig. 10 illustrates the diverse damage to the edge morphology of ceramics subsequent to the grinding of MgF_2 ceramics using various grinding wheels. By observing the edge of the workpiece in the direction of grinding, the most representative part was selected for discussion, with the degree of breakage being the maximum depth of the edge of the workpiece. Following the grinding processes employing structure 1~3 SFSGW, the edge of the workpiece exhibits varying degrees of fragmentation, with fragmentation depths measuring 42.33μm, 21.81μm, and 38.77μm, respectively. Notably, the edge of the workpiece exhibits the most severe damage following the grinding with structure 1 SFSGW. Conversely, the edge of workpiece morphology following USGW grinding exhibited the least damage, with a depth of only 6.28μm. Owing to their high hardness and low toughness, brittle hard materials are highly susceptible to cracking and crushing during the grinding processing. During the feeding process, the grinding wheel exerts significant compressive stress on the edge of MgF_2 ceramics. If the edge of the workpiece is unable to withstand this stress, it can lead to edge chipping and fracture. Structure 3 SFSGW has a smaller structured area compared to structure 2 SFSGW. Therefore, the grinding compressive stress on the workpiece of structure 3 SFSGW is more concentrated, and the depth of workpiece edge breakage is greater than that of the workpiece after grinding of structure 2 SFSGW. As grinding wheel wear continues to increase, worn abrasive grains may produce irregular cutting marks during the cutting process, and these marks may be more pronounced in the edge region of the workpiece, leading to increased edge damage.

In addition, edge fragmentation may be related to the structural integrity of the grinding wheel. A larger structured area increases the likelihood of contact between the edges of the structured grinding wheel grooves and the ceramic's edge during the feeding process, thereby causing damage to both the structured morphology of the biomimetic grinding wheel and the edge morphology of the material. Structure 1 SFSGW due to too large structuring area, the edge of the grinding wheel groove will continuously impact on the workpiece edge during the feeding process, and chipping phenomenon occurs. Therefore, an appropriate structured area can relatively reduce workpiece edge damage, while too large a structured area can exacerbate workpiece edge chipping. After experimental comparisons, it was found that structure 2 SFSGW resulted in relatively minimal damage depth to the edge morphology of the ceramic compared to the other two structures of the bionic grinding wheel.

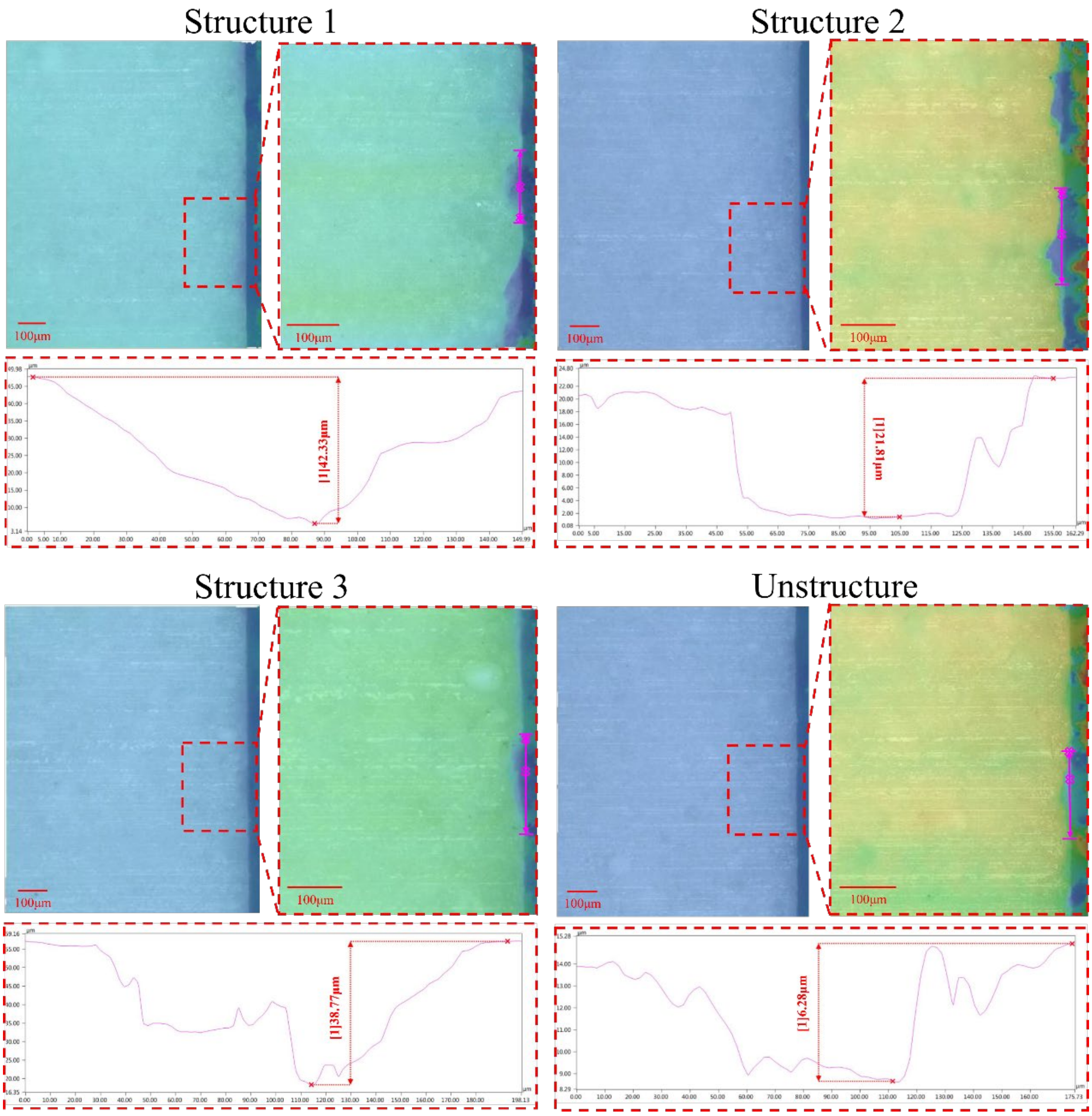

Fig. 10. Workpiece edge damage.

3.4 Grinding wheel wear

3.4.1 Morphology wear

The application of laser processing to bionic grinding wheels alters the overall wheel structure, resulting in higher surface pressure points compared to traditional grinding wheels (USGW). As the surface integrity of a grinding wheel decreases, the damage to its edges increases. Fig. 11 depicts noticeable edge chipping on the morphology of structure 1 SFSGW grinding wheel, whereas structure 2 and structure 3 SFSGW exhibit micro-wear and passivation. This phenomenon arises from the hindrance posed by the air barrier layer on the grinding wheel's surface. This barrier facilitates the preferential entry of grinding fluid into the grooves, causing grinding chips and fractured diamond grains to continuously impact the structural edges with the fluid. Bionic grinding wheels featuring an appropriate groove width can effectively lubricate the grinding region, thereby enhancing the lifespan and wear resistance of the abrasive particle when compare to traditional grinding wheels. However, excessively wide grooves in bionic grinding wheels can exacerbate grinding stresses, accelerate contour edge damage, and shorten grinding wheel service life.

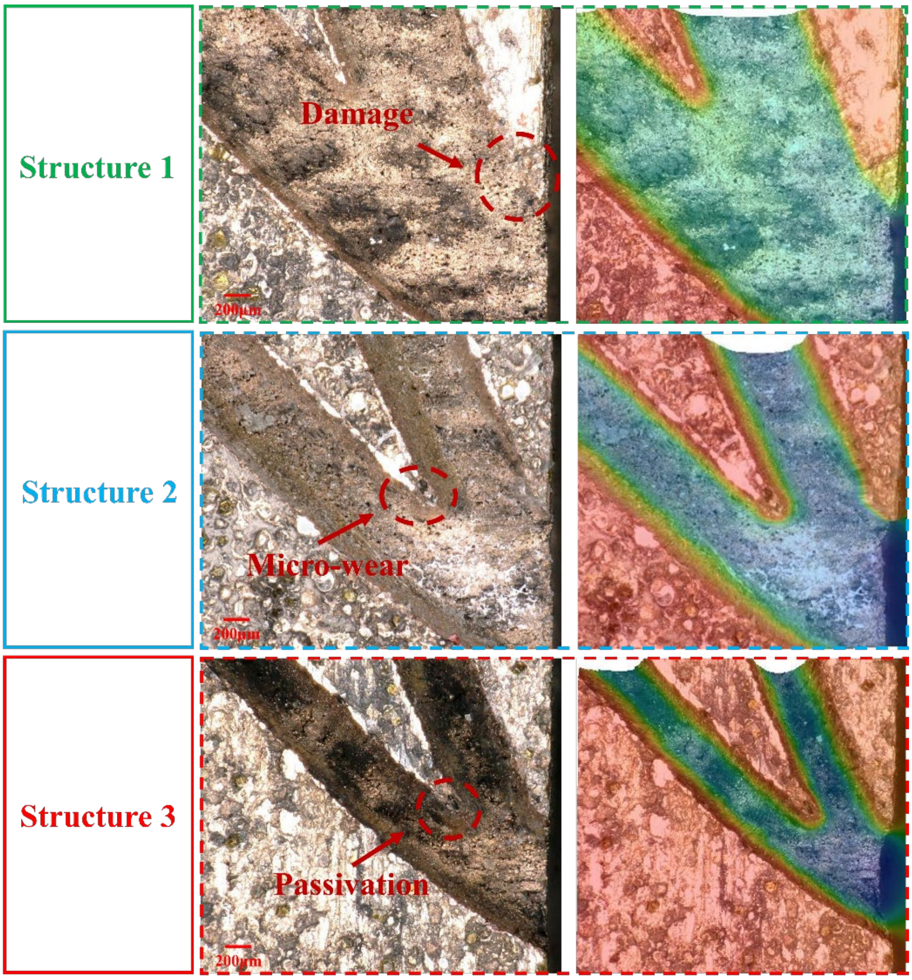

Fig. 11. Morphological damage to the grinding wheel edge after grinding.

3.4.2 Abrasive wear

The breakage of abrasive grains in the wheel is a pivotal factor influencing both the machining process (such as grinding force, grinding specific energy, etc.) and the resultant machining outcomes (including surface roughness and surface/subsurface damage). When machining brittle and hard materials, regions of high hardness on the workpiece induce mechanical wear on the abrasive particle. Excessive stress on the blade edge of the grit during grinding, surpassing its fracture strength, can result in rapid dulling or detachment of the grit. In the case of traditional grinding wheels, the high-speed friction between the wheel and the workpiece generates exceedingly high temperatures within the grinding zone. Unfortunately, the coolant is unable to effectively infiltrate this area, resulting in abrupt contact between the hot abrasive grains and the coolant. This sudden cooling induces thermal stresses in the grains exceeding their fatigue strength, thereby causing a part of grains fragmentation. Owing to the channeling effect of its grooves, the bionic designed shark fin-shaped grinding wheel facilitates the smooth flow of grinding fluid into the grinding region, thereby efficiently lowering the temperature within the grinding region. Fig. 12 illustrates the abrasive grains wear mechanism during the grinding process.

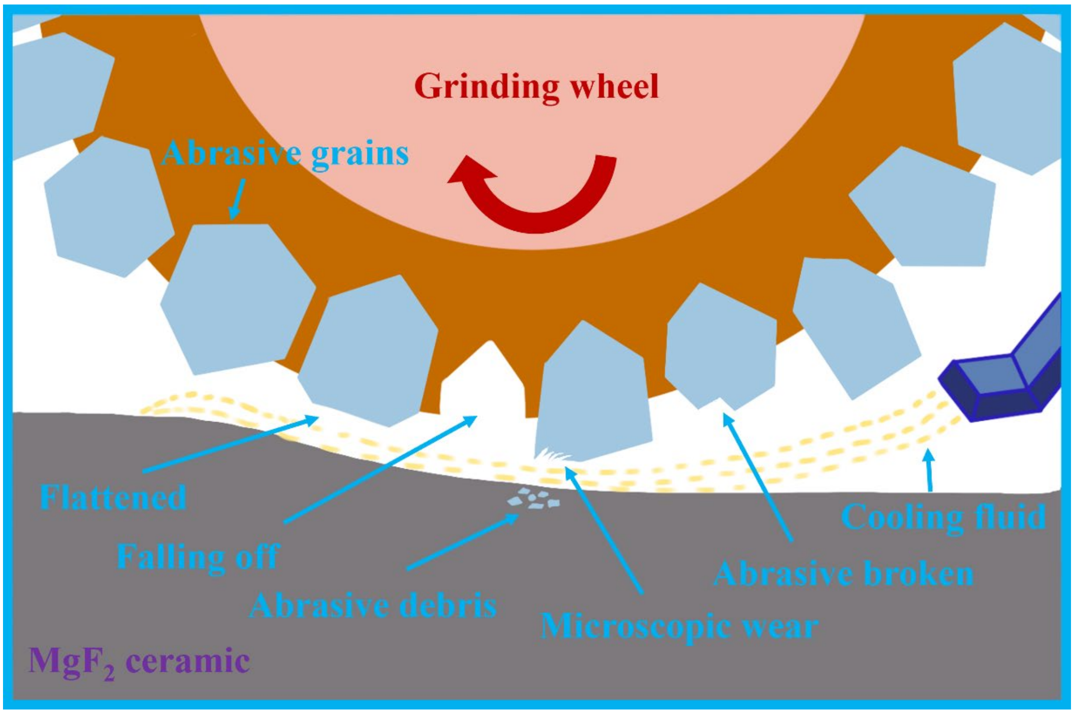

Fig. 12. Mechanism of abrasive grains wear.

Fig. 13 shows the abrasive grains breakage of USGW and three SFSGW with different groove widths before and after grinding MgF_2 ceramics. Firstly, in this experiment, the USGW and three kinds of SFSGW were observed by using ultra depth of field microscopy (ULDM), and several observation areas were selected and marked respectively. Then after a series of identical grinding experiments, the surface abrasive grains breakage in the marked areas of the four grinding wheels was observed. After the grinding experiments, some flattened and falling of abrasive grains occurred on the USGW. It can be observed that structure 1 SFSGW has relatively more severe abrasive grain destruction, with multiple flattening and shedding of abrasive grains. This is due to the fact that the number of abrasive grains that can be effectively processed by the structure 1 SFSGW is minimal, and the only remaining abrasive grains on the surface are repeatedly ground under tremendous grinding stresses, causing the grits to dull and fall off rapidly. Appropriate structuring of the grinding wheel surface can adequately lubricate the grinding area and reduce grinding heat and stress for the wheel abrasive grains, but too large an area of structuring can overload pressure on the effectively processed abrasive grains, and the degree of abrasive grains breakage can be even greater than that of conventional grinding wheels. Due to the small amount of structured area, the deflector characteristics of the structure 3 SFSGW are not sufficient to significantly improve the overall heat dissipation, which affects the durability of the abrasive grains, and the phenomenon of abrasive grains shedding occurs. However, the small amount of structuring resulted in a lower grinding force during grinding compared to conventional grinding wheels, so only a small amount of grit micro-wear was observed in structure 3 SFSGW. The experimental comparison shows that the degree of abrasive grains breakage of structure 2 SFSGW is the smallest, and thus it can also be introduced that structure 2 SFSGW has the best abrasion resistance.

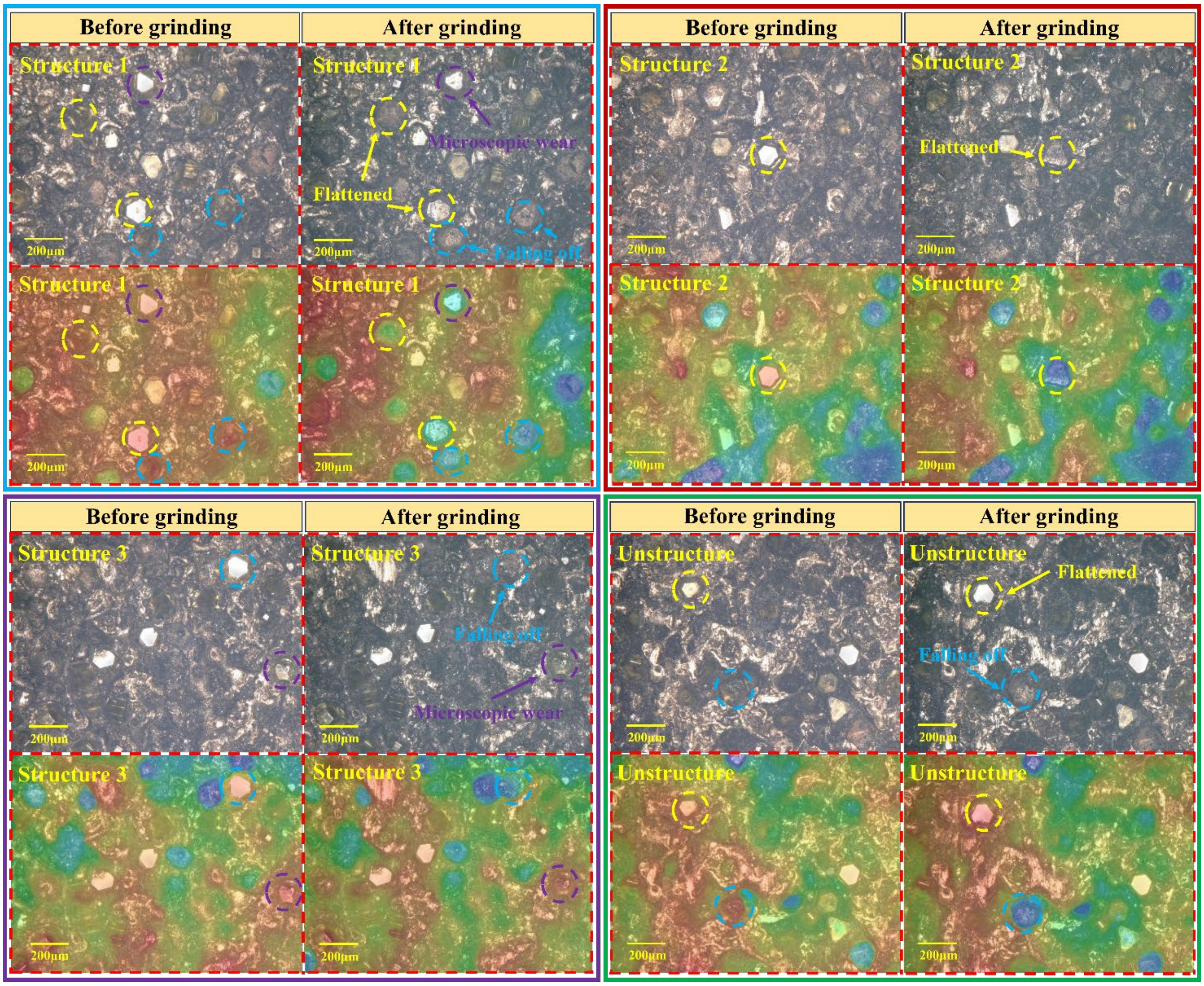

Fig. 13. Surface morphology of four different types of diamond grinding wheels before and after grinding MgF_2 ceramics.

4. Conclusion

In this paper, research on shark-fin bionic grinding wheels has advanced the in-depth understanding of abrasive grains-workpiece interactions in the grinding process and provided a theoretical basis for the optimization of the grinding process. Structured grinding wheels with bionics can improve grinding efficiency by optimizing the hydrodynamic characteristics and effectively suppressing the adverse effects of air turbulence on the grinding process. A new window material, MgF_2 ceramics, was machined using a bionic grinding wheel, and the grinding performance of the grinding wheel was discussed in terms of surface quality, surface roughness, and wheel grit wear mechanism. The main conclusions are drawn as follows:

1. The optimal laser parameters were selected through pre-experimentation and the designed shark-fin-like structure was precisely ablated on a bronze-bonded diamond grinding wheel. There is a part of molten metal attachment at the bottom of the groove, but the overall shape is intact, and there is no obvious crack or breakage at the edge part of the groove.

2. SFSGW effectively increases the efficiency of coolant utilization and reduces grinding temperatures. It makes the surface quality of MgF_2 ceramics effectively improved after grinding, but with the increase of structured area, the damage to the edge morphology of the workpiece is greater.

3. The excellent chip removal effect of the shark fin shape enables the grinding chips to be smoothly discharged with the coolant, reduces the damage to the workpiece, and effectively improves the surface roughness, and the surface roughness of the ground workpiece of structure 2 SFSGW is 22.15% lower than that of USGW.

4. Proper structuring of the grinding wheel can improve the grinding efficiency of the wheel, reduce the grinding stress and grinding heat of the wheel grits, and thus make the grinding wheel more resistant to wear. However, when the surface integrity factor of the grinding wheel is too small, the effective abrasive grains used for processing will be reduced, and the grinding force endured will increase sharply, thus increasing the abrasion of the grinding wheel and decreasing the effective service life of the grinding wheel. It was found that the grinding performance of the SFSGW with a slot width of 0.75 mm was significantly better than the other two SFSGWs.

Declaration of Competing Interest

The authors declare that they have no known competing financial interests or personal relationships that could have appeared to influence the work reported in this paper.

Acknowledgments

This project was sponsored by the National Natural Science Foundation of China (grant no. 52227809), the National Natural Science Foundation of China (grant no. 51875200), the Natural Science Foundation of Hunan Province (grant no. 2022JJ60085). Aid Program for Science and Technology Innovative Research Team in Higher Educational Institutions of Hunan Province (High Performance Manufacturing Processes and Service Performance Optimization).

References

[1] X. Liu, X. Wang, J. Zhu, J. Han, Thermal-mechanical response of microscale functional film for infrared window,

Transactions of Nonferrous Metals Society of China, 2014, 24(6):1791-1799.
https://doi.org/10.1016/S1003-6326(14)63255-6

[2] Z. Pan, X. Ma, H. Zhang, X. Li, M. Feng, L. Zhang, Investigation on Middle-Wave Infrared Window Materials for Hypersonic Application, Laser & Optoelectronics Progress, 2014, 51(9):91601.
https://doi.org/10.3788/lop51.091601

[3] P. Li, H. Wang, W. Wu, S. Ling, Process parameters optimization of Direct Synthesis Nano Magnesium Fluoride Powders, Applied Mechanics and Material, 2012, 184-185:1146-1149.
https://doi.org/10.4028/www.scientific.net/AMM.184-185.1146

[4] A. Nandiyatno, F. Iskandar, T. Ogi, K. Okuyama, Nanometer to submicrometer magnesium fluoride particles with controllable morphology, Langmuir, 2010, 26(14):12260.
https://doi.org/10.1021/la101194w

[5] P. Wan, C. Yuan, L. Tan, Q. Li, K. Yang, Fabrication and evaluation of bioresorbable PLLA/magnesium and PLLA/magnesium fluoride hybrid composites for orthopedic implants, Composites Science and Technology, 2014，98:36-43.
https://doi.org/10.1016/j.compscitech.2014.04.011

[6] X. Liu, B, Zhang, Grinding of nanostructural ceramic coatings: damage evaluation, International Journal of Machine Tools and Manufacture, 2003, 43(2):161-167.
https://doi.org/10.1016/S0890-6955(02)00157-8

[7] D. Wen, L. Wan, X. Zhang, C. Li, X. Ran, Z. Chen, Grinding performance evaluation of SiC ceramic by bird feather-like structure diamond grinding wheel, Journal of Manufacturing Processes, 2023, 95:382-391.
https://doi.org/10.1016/j.jmapro.2023.04.024

[8] N. Tala-Ighil, M. Fillon, P. Maspeyrot, Effect of textured area on the performances of a hydrodynamic journal bearing, Tribology International, 2011, 44(3):211-219.
https://doi.org/10.1016/j.triboint.2010.10.003

[9] Y. Henry, J. Bouyer, M. Fillon, An experimental analysis of the hydrodynamic contribution of textured thrust bearings during steady-state operation: a comparison with the untextured parallel surface configuration, Proceedings of the Institution of Mechanical Engineers, Part J: Journal of Engineering Tribology, 2015, 229(4):362-375.
https://doi.org/10.1177/1350650114537484

[10] C. Papadopoulos, E. Efstathiou, P. Nikolakopoulos, L. Kaiktsis, Geometry optimization of textured three-

dimensional micro-thrust bearings, Journal of Tribology, 2011, 133(4):041702.
https://doi.org/10.1115/1.4004990

[11] T. Enomoto, T. Sugihara, S. Yukinaga, K. Hirose, U. Satake, Highly wear-resistant cutting tools with textured surfaces in steel cutting, CIRP Annals, 2012, 61(1):571-574.
https://doi.org/10.1016/j.cirp.2012.03.123

[12] J. Deng, Z. Wu, Y. Lian, T. Qi, J. Cheng, Performance of carbide tools with textured rake-face filled with solid lubricants in dry cutting processes, International Journal of Refractory Metals and Hard Materials, 2012, 30(1):164-172.
https://doi.org/10.1016/j.ijrmhm.2011.08.002

[13] J. Kümmel, D. Braun, J. Gibmeier, J. Schneider, C. Greiner, V. Schulze, A. Wanner, Study on micro texturing of uncoated cemented carbide cutting tools for wear improvement and built-up edge stabilization, Journal of Materials Processing Technology, 2015, 215:62-70.
https://doi.org/10.1016/j.jmatprotec.2014.07.032

[14] W. Grabon, W. Koszela, P. Pawlus, S. Ochwat, Improving tribological behaviour of piston ring-cylinder liner frictional pair by liner surface texturing, Tribology International, 2013, 61:102–108.
https://doi.org/10.1016/j.triboint.2012.11.027

[15] W. Grabon, P. Pawlus, S. Wos, W. Koszela, M. Wieczorowski, Evolutions of cylinder liner surface texture and tribological performance of piston ring-liner assembly, Tribology International, 2018, 127:545-556.
https://doi.org/10.1016/j.triboint.2018.07.011

[16] S. Mezghani, I. Demirci, H. Zahouani, M. EI-Mansori, The effect of groove texture patterns on piston-ring pack friction, Precision Engineering, 2012, 36(2):210-217.
https://doi.org/10.1016/j.precisioneng.2011.09.008

[17] M. Wu, B. Guo, Q. Zhao, J. Zhang, High Efficiency Precision Grinding of Micro-structured SiC Surface Using Laser Micro-structured Coarse-Grain Diamond Grinding Wheel, International Journal of Precision Engineering and Manufacturing-Green Technology, 2019, 6(3):577-586.
https://doi.org/10.1007/s40684-019-00058-9

[18] B. Guo, M. Wu, Q. Zhao, H. Liu, J. Zhang, Improvement of precision grinding performance of CVD diamond wheels by micro-structured surfaces, Ceramics International, 2018, 44(14):17333-17339.
https://doi.org/10.1016/j.ceramint.2018.06.197

[19] Z. Chen, X. Zhang, D. Wen, S. Li, X. Wang, L. Gan, X. Rong, Improved grinding performance of SiC using an innovative bionic vein-like structured grinding wheel optimized by hydrodynamics, Journal of Manufacturing Processes, 2023, 101:195-207.
https://doi.org/10.1016/j.jmapro.2023.06.010

[20] Y. Liu, H. Zhang, P. Wang, Z. He, G. Dong, 3D-printed bionic superhydrophobic surface with petal-like microstructures for droplet manipulation, oil-water separation, and drag reduction, Materials & Design, 2022, 219:110765.
https://doi.org/10.1016/j.matdes.2022.110765

[21] G. Liu, Z. Yuan, Z. Qiu, S. Feng, Y. Xie, D. Leng, X. Tian, A brief review of bio-inspired surface technology and application toward underwater drag reduction, Ocean Engineering, 2020, 199: 106962.
https://doi.org/10.1016/j.oceaneng.2020.106962

[22] P. Ricco, M. Skote, M. Leschziner, A review of turbulent skin-friction drag reduction by near-wall transverse forcing, Progress in Aerospace Sciences, 2021, 123:100713.
https://doi.org/10.1016/j.paerosci.2021.100713

[23] J. Ye, M. Xu, P. Xing, Y. Cheng, D. Meng, Y. Tang, M. Zhu, Investigation of aerodynamic noise reduction of exterior side view mirror based on bionic shark fin structure, Applied Acoustics, 2021, 182:108188.
https://doi.org/10.1016/j.apacoust.2021.108188

[24] L. Wu, X. Liu, M. Wang, Effects of Bionic Volute Tongue on Aerodynamic Performance and Noise Characteristics of Centrifugal Fan Used in the Air-conditioner, Journal of Bionic Engineering, 2020, 17(4):780-792.
https://doi.org/10.1007/s42235-020-0067-7

[25] Y. Zhang, Z. Pan, Z. Gu, S. Liu, A Research on Bionic Aerodynamic Drag Reduction of Vehicle Body Based on Shark Fins, Automotive Engineering, 2017, 39(9):1018-1024 and 1029.
https://doi.org/10.19562/j.chinasae.qcgc.2017.09.007

[26] C. Wei, Z. Wei, X. Chen, K. He, Structural Design of a Bionic Anti-Clogging Drip Irrigation Emitter Based on Shark Dorsa Fin, Journal of Geoscience and Environment Protection, 2021, 09(4):11-20.
https://doi.org/10.4236/gep.2021.94002

[27] H. Yang, B. Wang, L. Ma, Mechanical properties of 3D double-U auxetic structures, International Journal of Solids and Structures, 2019, 180/181:13-29.
https://doi.org/10.1016/j.ijsolstr.2019.07.007

[28] S. Liu, C. Lü, Y. Rao, S. Wang, Performance Analysis and Research of Shark Fin Structure Based Performance Analysis and Research of Shark Fin Structure Based on Simulation, Journal of System Simulation, 2018, 30(6):2398-2404.
https://doi.org/10.16182/j.issn1004731x.joss.201806050

[29] W. Zhou, G. Chen, H. Pan, F. Luo, Y. Wei, M. Li, Laser precision profiling of small-angle bevel-edge contour grinding wheels, Journal of Materials Processing Technology, 2022, 305:117591.
https://doi.org/10.1016/j.jmatprotec.2022.117591

[30] H. Deng, C. He, W. Liu, W. Xiong, Trajectory planning of deep-cutting laser profiling of superabrasive profile grinding wheels, Engineering Science and Technology, an International Journal, 2023, 48: 101581.
https://doi.org/10.1016/j.jestch.2023.101581

[31] H. Deng, G. Chen, J. He, C. Zhou, H. Du, Y. Wang, Online, efficient and precision laser profiling of bronze-bonded diamond grinding wheels based on a single-layer deep-cutting intermittent feeding method, Optics & Laser Technology, 2016, 80:41-50.
https://doi.org/10.1016/j.optlastec.2015.12.021